6th European Conference on Computational Mechanics (ECCM 6)
7th European Conference on Computational Fluid Dynamics (ECFD 7)
1115 June 2018, Glasgow, UK

SIMULATION OF UPPER AND LOWER BAINITIC TRANSFORMATION IN A UNIFIED PHASE FIELD MODEL

ROLF MAHNKEN[1] AND MARTIN DÜSING[2]

[1] Chair of Engineering Mechanics, Paderborn University
Warburger Straße 100, 33098 Paderborn, Germany
mahnken@ltm.upb.de

[2] Chair of Engineering Mechanics, Paderborn University
Warburger Straße 100, 33098 Paderborn, Germany
duesing@ltm.upb.de

Key words: Bainite, Diffusion, Phase field method, Cahn-Hilliard, Ginzburg-Landau

Abstract. In materials science one distinguishes between upper and lower bainite. Both microstructures develop due to different diffusion processes depending on the isothermal process temperature. In this work we describe these different mechanisms with a new diffusion model coupled to a multiphase-field equation. Numerical examples demonstrate the expected behaviour.

1 INTRODUCTION

Bainite is a steel microstructure consisting of the three phases bainitic ferrite, carbides and (residual) austenite which form the two morphologies upper and lower bainite [3]. Both transitions start with a displacive transformation from austenite to bainitic ferrite which does not depend on the carbon diffusion and therefore lead to a supersaturated bainitic ferrite phase. The subsequent diffusion is highly dependent on the transformation temperature. At high temperatures the carbon atoms succeed in leaving the supersaturated bainitic ferrite into the austenite phase where carbides will precipitate if the carbon concentration is high enough. The resulting morphology is called upper bainite. Whereas in lower bainite, only a minor part of the carbon atoms, those who are already near the interface, succeed in leaving the bainitic ferrite while most of the carbon stays within the bainitic ferrite to build accumulations [3]. At these accumulations carbides precipitate.

2 A DIFFUSION MODEL FOR UPPER AND LOWER BAINITE

The main challenge of modelling the formation of both morphologies, upper and lower bainite, are the different diffusion mechanism of carbon. To this end as a model assumption, three different diffusion processes are introduced which are involved for upper and lower bainite [4]. These diffusion types are illustrated in Figure 1 and henceforth denoted as Type I, Type II and Type III, respectively [4]. All three types are described on domains

with two phases coloured in red and yellow and diffuse interfaces in between, which are illustrated by black dashed lines. In this work a phase field method is used to distinguish different phases. A fundamental property of this method are diffuse interfaces between phases. Therefore the diffusion model considers diffuse interfaces between phases.

I. *Separation*: The separation process takes place within one phase. In Figure 1.I the carbon atoms, illustrated as black dots separate within the red phase. The process leads to accumulations of carbon at a high concentration limit surrounded by an area at a low concentration limit.

II. *Accumulation*: The diffusion process described in Figure 1.II shows an accumulation of carbon atoms within the interface. The initially uniformly distributed atoms are transported to one specific side of the diffuse interface, thus resulting into a non-uniform distribution [4].

III. *Balancing*: The balancing mechanism describes a very basic diffusion process. Starting with a non-uniform distribution the balancing mechanism leads to a uniform distribution. This movement can be observed in Figure 1.III for both phases which are treated separately. The concentrations in different phases may differ. For the specific case in Figure 1.III, the balancing process especially moves carbon atoms which are accumulated within the interface but close to the bulk phase, into the bulk phase, while on the other side of the interface it pushes atoms into the empty interface [4].

Diffusion across the interface is achieved combining accumulation within an interface (Type II) with the balancing process (Type III). While Type II arranges the accumulation within the interface, Type III governs the flow into and out of the interface region.

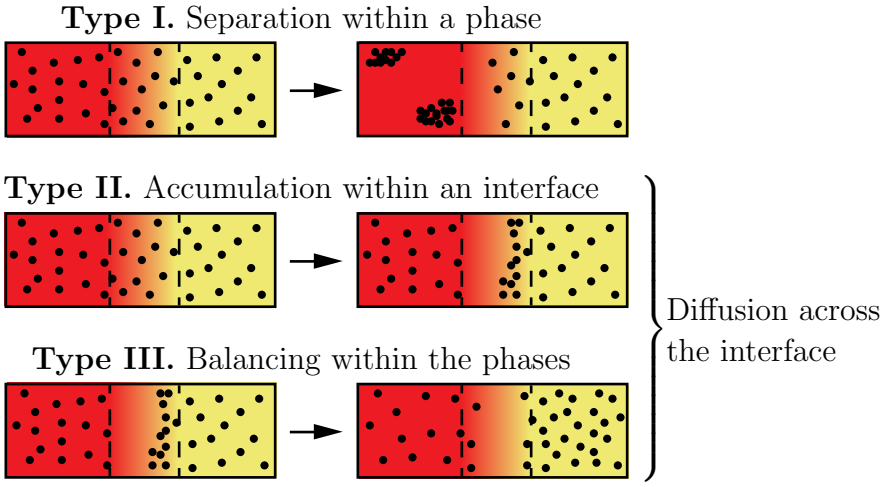

Figure 1: Schematics of three diffusion mechanisms [4]

The mechanisms of separation within a phase (Type I) takes place only within bainitic ferrite of lower bainite. Here it is the most important diffusion process because it leads to the precipitation of carbides within the bainitic ferrite, which is the typical pattern of this morphology.

The accumulation process within an interface (Type II) happens in both upper and lower bainite between the bainitic ferrite and the austenite phases. This is the major diffusion process in upper bainite while it plays a minor role in lower bainite. Furthermore in upper bainite carbon diffuses from the austenite into the carbide. The nucleating carbides attract surrounding carbon to grow faster and stabilize itself [4].

Type III diffusion, the balancing within the phases is needed to assist the diffusion across the interface between bainitic ferrite and austenite. However it is not needed in bainitic ferrite in lower bainite, because here the separation within a phase (Type I) governs the carbon movement and guarantees a minor flow into the interface.

The phase transformation from austenite to bainitic ferrite is independent from the carbon diffusion which is a subsequent process governing the precipitation of carbides and the growth of residual austenite. The transformation from austenite to bainitic ferrite is therefore called displacive. The precipitation of carbides is mainly influenced by the carbon concentration for both morphologies, upper and lower bainite.

The interface width shown in Figure 1 and the one used for the following phase field model is oversized due to computational limits. Nevertheless, the diffusion mechanism does not depend on the interface width [4].

3 A PROTOTYPE MODEL FOR UPPER AND LOWER BAINITE

The governing equations of the thermodynamic framework in [2] are specified in this section for a combined model for upper and lower bainite. Therefore we introduce the following order parameters:

I. Bainitic ferrite: ϕ_1,

II. Austenite: ϕ_2,

III. Carbide: ϕ_3

and c describes the carbon concentration.

3.1 Weighted Helmholtz energy

The Helmholtz energy function is a major instrument to capture the different diffusion mechanisms of Figure 1 for bainite [4]. It is postulated as a sum of two energies

$$\hat{\psi}(\tilde{\boldsymbol{z}}) = \hat{\psi}_c(c, \nabla c) + \hat{\psi}_\phi(c, \phi_1, \phi_2, \phi_3, \nabla\phi_1, \nabla\phi_2, \nabla\phi_3), \tag{1}$$

with part $\hat{\psi}_c$ considering the diffusion which is only a function of $c, \nabla c$ and a phase-field part $\hat{\psi}_\phi$ which includes coupling terms as it is a function of $c, \phi_1, \phi_2, \phi_3, \nabla\phi_1, \nabla\phi_2, \nabla\phi_3$. The function $\hat{\psi}_c(c, \nabla c)$ is a sum of two energies

$$\hat{\psi}_c(c, \nabla c) = w_f(\theta)\hat{\psi}_f(c) + w_s(\theta)\hat{\psi}_s(c, \nabla c). \tag{2}$$

The first summand including the energy term $\hat{\psi}_f(c)$ accounts for the balancing diffusion (Type III) according to Figure 1.III, which will result into Fick's type of diffusion [4], whereas $\hat{\psi}_s(c, \nabla c)$ governs the separation of carbon (Type I) according to Figure 1.I. The carbon in upper bainite diffuses across the interface Type (II+III) into the austenite phase while in lower bainite the diffusion across the interface is of minor importance compared to the separation (Type I) as explained in Section 2. This combined effect is accounted for by weighting functions w_f and w_s, respectively, in equation (2). The different diffusion mechanism are weighted to distinguish upper from lower bainite and therefore are dependent on the temperature θ. Both weighting functions are illustrated in Figure 2 versus the temperature θ and are defined as

$$w_f(\theta) = \begin{cases} 0 & \text{for } \theta < \theta_D - \varepsilon_\theta \\ 1 & \text{for } \theta > \theta_D + \varepsilon_\theta \\ \dfrac{1}{2} + \dfrac{L_D}{2} + \left(\dfrac{1}{2} - \dfrac{L_D}{2}\right) \sin\left(\pi \left(\dfrac{\theta - \theta_D}{2\varepsilon_\theta} + 2\right)\right) & \text{otherwise} \end{cases} \tag{3}$$

and

$$w_s(\theta) = \begin{cases} 1 & \text{for } \theta < \theta_D - \varepsilon_\theta \\ 0 & \text{for } \theta > \theta_D + \varepsilon_\theta \\ \dfrac{1}{2} - \dfrac{L_D}{2} + \left(\dfrac{1}{2} - \dfrac{L_D}{2}\right) \sin\left(\pi \left(\dfrac{\theta - \theta_D}{2\varepsilon_\theta} + 1\right)\right) & \text{otherwise.} \end{cases} \tag{4}$$

The isothermal transformation temperature is denoted as θ, the transition temperature θ_D marks the boundary between upper and lower bainite, ε_θ is a factor to soften the sharp boundary for better numerical characteristics and L_D ensures the coaction of both diffusion mechanisms in lower bainite. Both functions w_f and w_s satisfy the completeness condition [4]

$$w_f(\theta) + w_s(\theta) = 1. \tag{5}$$

For the separation (Type I) in lower bainite a Cahn-Hilliard type equation is implemented. The corresponding Helmholtz energy reads

$$\hat{\psi}_s(c, \nabla c) = f(c) + \frac{1}{2}\rho |\nabla c|^2, \tag{6}$$

$$f(c) = d(c_{\text{eq}} - c)^2 (c_{\text{carb}} - c)^2. \tag{7}$$

where ρ is a Cahn-Hilliard balance factor, the double well energy function is denoted as $f(c)$, with turning points at c_{eq} which is the equilibrium carbon concentration in bainitic ferrite and c_{carb} which is the carbon concentration of the carbides. These two concentrations define the limits of the separation process [4].

For the balancing Fick's diffusion (Type III) a different Helmholtz energy is required

$$\hat{\psi}_f(c) = \frac{c_{\text{eq}} \ln(c_{\text{eq}} - c) - c_{\text{carb}} \ln(c_{\text{carb}} - c) + c \ln(\frac{c_{\text{carb}} - c}{c_{\text{eq}} - c})}{c_{\text{eq}} - c_{\text{carb}}}. \tag{8}$$

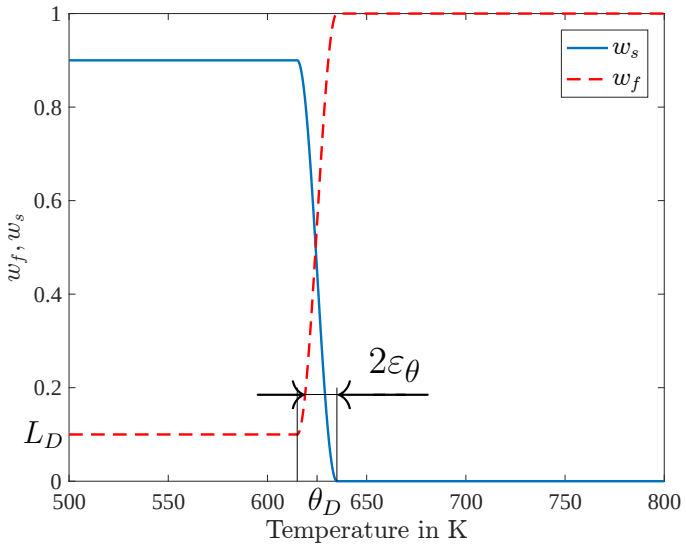

Figure 2: Weighting functions for different diffusion processes [4]

Equation (8) is a modification of Wheeler et al. [5], where the original bounds 0 and 1 are replaced with c_{carb} and c_{eq} [4]. The derivation from equation (8) to Fick's type diffusion within the framework used in this work is described in the Appendix of [4].

The Helmholtz energy for the phase transformation in equation (1) is postulated as

$$\hat{\psi}_\phi(c, \phi_1, \phi_2, \phi_3, \nabla\phi_1, \nabla\phi_2, \nabla\phi_3) = \sum_{i=1}^{N_p} \sum_{j>i}^{N_p} \frac{1}{q_{ij}} \left[h_{kj}(\phi_i, \phi_j, \nabla\phi_i, \nabla\phi_j) + (1 + c\ s_{ij}\ w_f)\ g_{kj}(\phi_i, \phi_j) \right] \quad (9)$$

where $h_{kj}(\phi_i, \phi_j, \nabla\phi_i, \nabla\phi_j)$ is the interfacial energy density and $g_{kj}(\phi_i, \phi_j)$ the potential energy between two phases i and j. The phase energy coefficients are denoted by q_{ij}. The additional term $c\ s_{ij}\ w_f$ is introduced, where s_{ij} are interface diffusion factors which govern the accumulation of carbon within the interface (Type II) between phases i and j according to Figure 1.II [4]. Following [6], the interfacial energy density is chosen as

$$h_{kj}(\phi_i, \phi_j, \nabla\phi_i, \nabla\phi_j) = \frac{1}{2}\alpha_{ij}(\phi_j \nabla\phi_i - \phi_i \nabla\phi_j)^2 \quad (10)$$

where α_{ij} is a phase gradient energy coefficient. The chemical or potential energy density g_{kj} between two phases i and j is proposed as a simple double well potential [1]

$$g_{kj}(\phi_i, \phi_j) = \frac{1}{4a_{ij}} \phi_i^2 \phi_j^2, \quad (11)$$

where the potential constants are denoted as a_{ij}.

3.2 Evolution equations

In order to gain the evolution equations for the concentration field c and the phase order parameters ϕ_i, the constitutive moduli $\beta\,\tau, \beta_i$ and the mobility tensor $\boldsymbol{A}$ introduced in [2] have to be specified. Constant moduli are postulated

$$\tau(\boldsymbol{z}) = \tau w_s = \text{const.}, \tag{12}$$

$$\beta_i(\boldsymbol{z}) = \beta_i = \text{const.} \tag{13}$$

In order to account for both, separation within a phase (Type I) and diffusion across the interface (Type II + Type III), the mobility tensor $\boldsymbol{A}$ is postulated as the sum of two terms, weighted by w_f and w_s introduced in equations (3) and (4) [4],

$$\boldsymbol{A}(\boldsymbol{z}) = \left(w_f D_f(\phi) f_q(c) + w_s D_s(\phi)\right) \mathbf{1}, \tag{14}$$

with

$$D_f(\phi) = \sum_{i=1}^{N_p} \phi_i D_{fi}, \tag{15}$$

$$D_s(\phi) = \sum_{i=1}^{N_p} \phi_i D_{si} \tag{16}$$

$$f_q(c) = (c - c_{\text{eq}})(c_{\text{carb}} - c). \tag{17}$$

In equations (15) and (16) the diffusion coefficients for diffusion across the interface and Cahn-Hilliard diffusion are denoted as D_{fi} and D_{si}, respectively.

In the next step the evolution equations can be assembled using the constitutive equations. The weighted chemical potential reads

$$\mu = w_f \mu_f + w_s \mu_s, \tag{18}$$

where

$$\mu_f = \frac{\partial \hat{\psi}_f(c)}{\partial c} + \sum_{i=1}^{N_p} \sum_{j>i}^{N_p} v_{ij} \phi_i^2 \phi_j^2, \tag{19}$$

$$\mu_s = \frac{\partial f}{\partial c} - \rho \Delta c + \tau \dot{c}. \tag{20}$$

and for brevity

$$v_{ij} = \frac{s_{ij}}{4 a_{ij} q_{ij}}. \tag{21}$$

The evolution equation for the concentration field c renders [4]

$$\dot{c} = \nabla \cdot (w_f \boldsymbol{A}(\boldsymbol{z}) \cdot \nabla \mu_f) + \nabla \cdot (w_s \boldsymbol{A}(\boldsymbol{z}) \cdot \nabla \mu_s). \tag{22}$$

In the next step only μ_f from equation (19) is inserted into equation (22) in order to avoid fourth order derivatives in the evolution equation of c which would occur inserting μ_s (20) as well. Fourth order derivatives would lead to difficulties for the finite element implementation, described in the next section [4].

The term $\boldsymbol{A}(\boldsymbol{z})\cdot\nabla\mu_f$ in equation (22) leads to simplifications in the resulting equation. The lengthy algebra describing the steps in detail can be found in the Appendix of [4]. The partial differential equation of the concentration field c renders

$$\begin{aligned}\dot{c} = {} & w_f^2\nabla D_f(\phi)\cdot\nabla c + w_f^2 D_f(\phi)\Delta c + w_s w_f \nabla D_s(\phi)\frac{\partial^2\hat{\psi}_f(c)}{\partial c^2}\nabla c \\ & + w_s w_f D_s(\phi)\frac{\partial^3\hat{\psi}_f(c)}{\partial c^3}(\nabla c)^2 + w_s w_f D_s(\phi)\frac{\partial^2\hat{\psi}_f(c)}{\partial c^2}\Delta c \\ & + \left(w_f^2\nabla D_f(\phi) f_q(c) + w_f^2 D_f(\phi)\frac{\partial f_q(c)}{\partial c}\nabla c + w_s w_f \nabla D_s(\phi)\right) \\ & \cdot \sum_{i=1}^{N_p}\sum_{j>i}^{N_p} v_{ij}\left(2\phi_i\phi_j^2\nabla\phi_i + 2\phi_j\phi_i^2\nabla\phi_j\right) \\ & + \left(w_f^2 D_f(\phi) f_q(c) + w_s w_f D_s(\phi)\right) \\ & \sum_{i=1}^{N_p}\sum_{j>i}^{N_p} 2v_{ij}\left(\nabla\phi_i\phi_j^2\nabla\phi_i + \nabla\phi_j\phi_i^2\nabla\phi_j + 4\phi_i\phi_j\nabla\phi_i\nabla\phi_j + \phi_j\phi_i^2\Delta\phi_j + \phi_i\phi_j^2\Delta\phi_i\right) \\ & + \left(w_s w_f \nabla D_f(\phi) f_q(c) + w_s w_f D_f(\phi)\frac{\partial f_q(c)}{\partial c}\nabla c + w_s^2\nabla D_s(\phi)\right)\cdot\nabla\mu_s \\ & + \left(w_s w_f D_f(\phi) f_q(c) + w_s^2 D_s(\phi)\right)\Delta\mu_s \end{aligned} \quad (23)$$

The partial differential equations for the phase order parameters ϕ_i read

$$\dot{\phi}_i = \sum_{j=1, j\neq i}^{N_p}\frac{1}{\beta_i q_{ij}}\left(\alpha_{ij}\left(\phi_j\Delta\phi_i - \phi_i\Delta\phi_j\right) - \frac{\phi_i\phi_j\cdot(1 + c\ s_{ij}\ w_f)}{2a_{ij}}(\phi_j - \phi_i)\right) + \gamma_i, \quad \text{for} \quad i = 1, ..., N_p\ . \quad (24)$$

In a next step the constant material parameters are changed according to [7] for a better physical interpretation. The phase gradient energy coefficients α_{ij}, the potential constants a_{ij}, the phase energy coefficients q_{ij} and the dissipative moduli β_i of equation (24) are replaced by the interface mobilities ζ_{ij}, interface energies σ_{ij} and interface thicknesses η_{ij}

$$\beta_i q_{ij} = \frac{\eta_{ij}}{\zeta_{ij}}, \qquad a_{ij} = \frac{\eta_{ij}}{72\sigma_{ij}}, \qquad \alpha_{ij} = \sigma_{ij}\eta_{ij}. \quad (25)$$

For details on the external forces γ_i of equation (24) and the carbide precipitation see [2].

The evolution equation for the phase order parameters (24) can now be written as

$$\dot{\phi}_i = \sum_{j=1,j\neq i}^{N_p} \zeta_{ij} \left[\sigma_{ij} \left((\phi_j \Delta\phi_i - \phi_i \Delta\phi_j) - \frac{36}{\eta_{ij}^2} (1 + c\ s_{ij}\ w_f) \phi_i \phi_j (\phi_j - \phi_i) \right) - \frac{6 \Delta G_{ij}(\boldsymbol{z})}{\eta_{ij}} \phi_i \phi_j \right]$$
$$\text{for} \quad i = 1, ..., N_p. \quad (26)$$

4 NUMERICAL IMPLEMENTATION

This section documents the implementation of the coupled set of the partial differential equations (20), (23) and (26). To find a solution μ_s, c, ϕ_i on a two-dimensional domain B for specific boundary and initial conditions in the time period $[0, T]$ the finite element method is used. Quadrilateral elements with linear shape functions are used for the finite element formulation while the backward Euler method is applied for the time derivatives. The resulting algebraic system of equations is solved with Newton's method [4].

As mentioned in Section 3.2 the chemical potential μ_s for the lower bainitic transformation is handled as a separate degree of freedom to avoid fourth order derivatives and not inserted into the evolution equation of the concentration (23) [4]. The five unknowns per finite element node are $c, \mu_s, \phi_1, \phi_2, \phi_3$. Details can be found in [4].

5 REPRESENTATIVE EXAMPLES

Two examples, one for upper and one for lower bainitic transformation, are presented in this section. They are based on the framework described in [2] and the constitutive equations introduced in Section 3. The implementation described in the previous section is used here. Both examples are simulated with the finite element method on a domain of 3 µm × 3 µm subdivided into 16384 quadrilateral elements. Homogeneous Neumann boundary conditions are prescribed for all variables as

$$\bar{\mu} = 0, \quad \bar{c} = 0, \quad \bar{\phi}_i = 0. \quad (27)$$

The initial carbon concentration $c(t = 0) = c_0$ is set to $c_0 = 1.87$ wt.% with small random perturbations. The carbide phase has small random perturbations between $\phi_{30} = 0$ and $\phi_{30} = 0.01$ which are uniformly distributed.

The total time of the simulation is set to $T = 0.03$ s with a the time step size of $\Delta t = 0.00001$ s. In Table 2 in [4] the material parameters are summarized. The material parameters for upper and lower bainite are the same, in order to highlight differences in the diffusion mechanisms.

5.1 Upper bainite transformation

The first example shows a simulation for an upper bainite transformation at $\theta = 700$ K. The results are illustrated in Figure 3. The first column at 0 s represents the initial conditions. The austenite phase ϕ_2 in Figure 3.a dominates the domain at the beginning. Only two nuclei of bainitic ferrite ϕ_1 on the left boundary penetrate the austenite phase (Figure 3.b). There are no carbides (Figure 3.c) at the beginning beside the very small

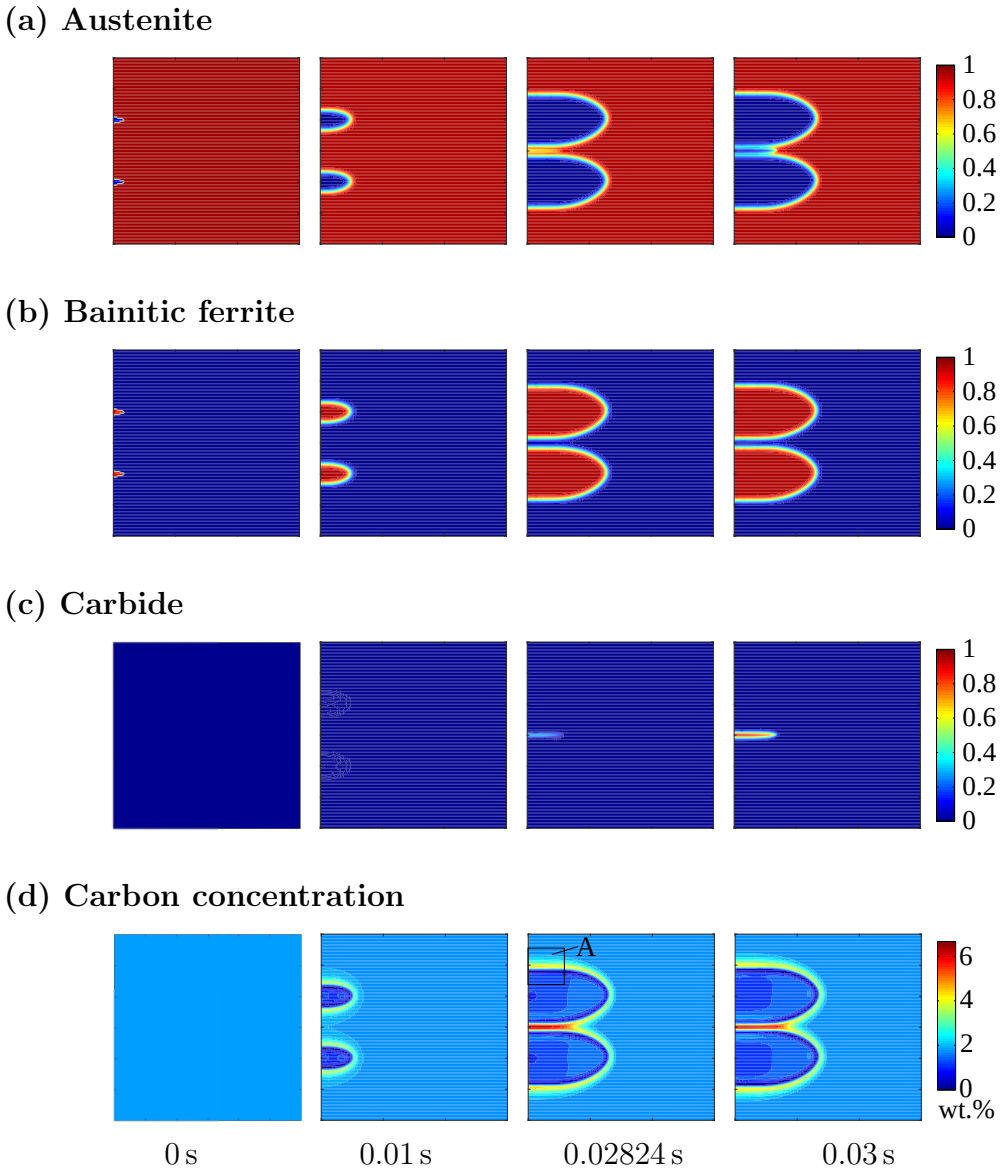

Figure 3: Upper bainitic transformation at 0 s, 0.01 s, 0.02824 s and 0.03 s. [4]

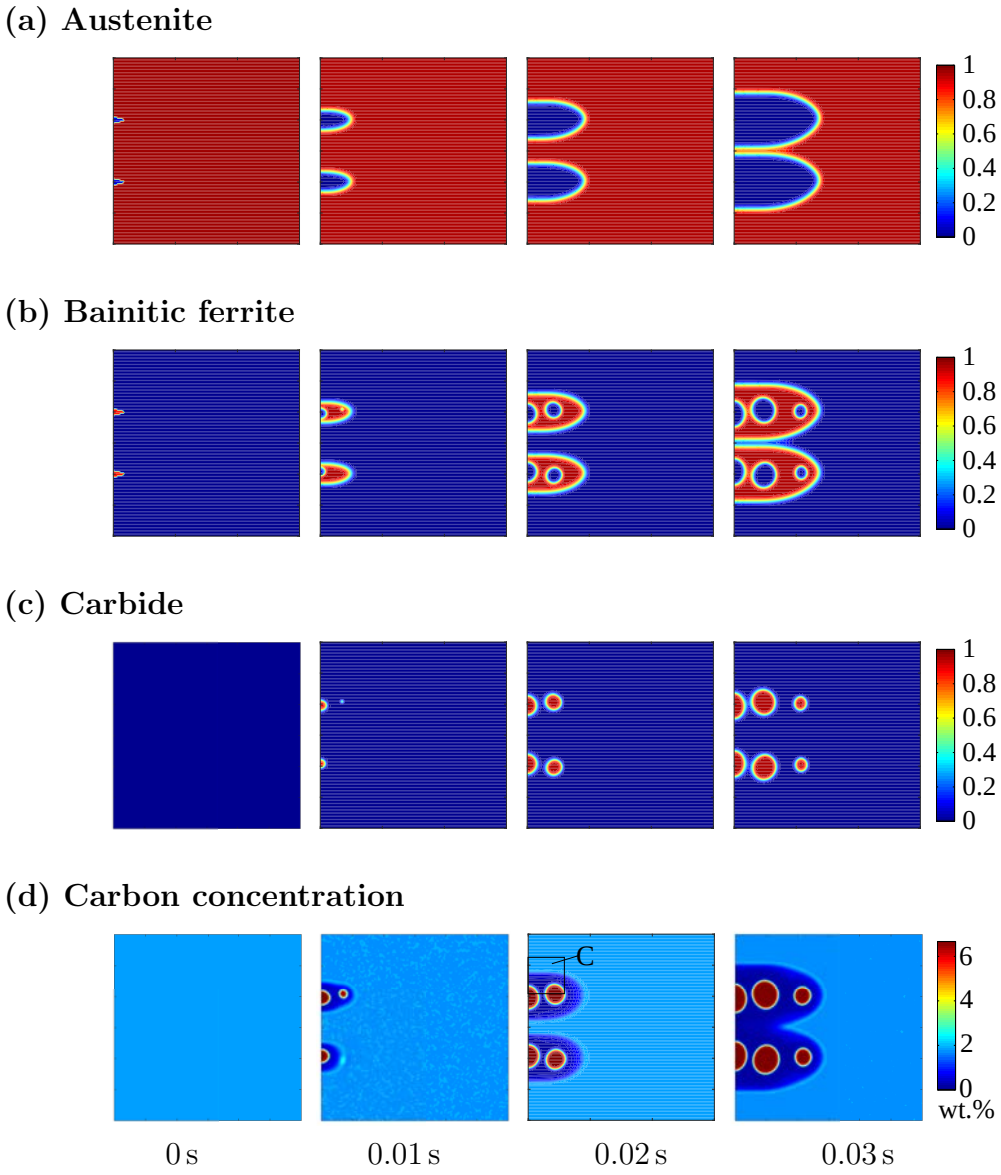

Figure 4: Lower bainitic transformation at 0 s, 0.01 s, 0.02 s and 0.03 s. [4]

initial perturbations, described above, which are too small to be visible in this diagram. The next step shown is at $t = 0.01\,\mathrm{s}$. The bainitic ferrite phase is larger and the diffuse interface, which is typical for phase field models, can be seen between austenite and bainitic ferrite. There is still carbide phase at this time. The carbon concentration (Figure 3.d), which is initially equally distributed shows major changes. The concentration within the bainitic ferrite decreased noticeably while the carbon moves across the interface to accumulate directly behind the interface within the austenite phase. This process is described in Section 2 as diffusion across the interface, where Type II diffusion, as the major player, works within the interface between bainitic ferrite and austenite, while Type III diffusion ensures a flow from the bainitic ferrite into the interface. The new gradient of carbon concentration within the austenite phase leads to a balancing diffusion effect (Type III) within the austenite. Carbon atoms are transported from the accumulations to areas of lower concentration. This process happens subsequently after the phase transformation from austenite to bainitic ferrite. At $t = 0.02824\,\mathrm{s}$ both bainitic ferrite sheaves are larger than before. In between these sheaves the carbon concentration reaches a its maximum of $c = 6.67\,\mathrm{wt.\%}$, so that carbides ϕ_3 precipitate. This can be seen in Figure 3.c at $t = 0.02824\,\mathrm{s}$. The precipitation of carbides is self-enhancing, because the carbide phase pulls the surrounding carbon into the carbide phase which enforces the growth of the carbide [4]. The carbide phase limits the growth of the bainitic ferrite phase.

5.2 Lower bainite transformation

The lower bainitic transformation is simulated in the second example at $\theta = 600$ K. The initial conditions in the first column of Figure 4 are same as in the previous example. There are two nuclei of bainitic ferrite ϕ_1 on the left boundary while the rest of the domain is austenitic ϕ_2. Both nuclei grow during the ensuing time steps. The growth is displacive and faster than any diffusion of carbon. Therefore the bainitic ferrite is supersaturated. To minimize the energy the carbon starts to move. Most of the carbon c stays within the bainitic ferrite ϕ_1, because of the lower temperature and the likewise slower diffusion speed [4]. The carbon starts to build accumulations. It can be seen that these accumulations grow in time. At these accumulations carbides will precipitate if the concentration reaches it maximum of $c = 6.67\,\mathrm{wt.\%}$. The precipitation process takes place within the bainitic ferrite in this example for lower bainite in contrast to upper bainite, where the carbides grow within the austenite phase. However like in the previous example for upper bainite, some carbon succeed in leaving the supersaturated bainitic ferrite in lower bainite, too and move across the interface into the austenite phase.

6 CONCLUSIONS

The numerical examples show the expected behaviour described in the Introduction. The three different diffusion mechanism are successfully combined with weighting functions to simulate upper and lower bainite depending on the temperature. Furthermore the precipitation of carbides is simulated at carbon accumulations within bainitic ferrite and austenite.

REFERENCES

[1] M. Düsing and R. Mahnken, *Comp. Mater. Sci.* (2016) **111**:91–100.

[2] M. Düsing and R. Mahnken, *Arch. Appl. Mech.* (2016) **86**(12):1947–1964.

[3] H.K.D.H. Bhadeshia, *Bainite in steels*, Maney Materials Science, Cambridge, 2nd Edition, 2001.

[4] M. Düsing and R. Mahnken, *Int. J. Solids Struct.* (2018) **135C**:172–183.

[5] A. A. Wheeler, W. J. Boettinger, G. B. McFadden, *Physical Review A* (1992) **45**(10):7424–7439.

[6] I. Steinbach, F. Pezzolla, B. Nestler, M. Seeßelberg, R. Ptieler, G.J. Schmitz, J.L.L. Rezende, *Physica D* (1996) **94**:135–147.

[7] M.G. Mecozzi, J. Sietsma, S. van der Zwaag, M. Apel, P. Schaffnit, I. Steinbach, *Metallurgical and Materials Transactions A* (2005) **36A**:2327–2340.